10

Vircators, Gyrotrons and Electron Cyclotron Masers, and Free-Electron Lasers

10.1 Introduction

This chapter is devoted to a somewhat briefer treatment of three classes of narrowband microwave sources that are unrelated in their underlying operating principles: virtual cathode oscillators, gyrotrons and electron cyclotron masers, and free-electron lasers. The reason for collecting these microwave sources in a single chapter is that at this time we regard these three classes of narrowband sources as somehow less significant in the field of high power microwaves (HPM) than the sources of Chapters 7 to 9. Let us consider each separately and state the reasons for our admittedly subjective judgment, which varies with the source, recognizing that the significance of any one of them could change with shifts in the technology or application needs.

Virtual cathode oscillators are enjoying something of a renaissance at this time, and developments with two variants in particular — tunable vircators and coaxial vircators — may yet overcome two problems that have plagued devices of this type: low efficiency and sensitivity to gap closure in the high-current, explosive emission diodes that are so often used with sources of this type. Nevertheless, despite their efficiency problems, these sources are attractive in applications requiring a simple source configuration — vircators many times employ no applied magnetic field and no slow-wave structure — and low device impedance, which permits high power operation at low voltage or optimizes coupling with low-impedance power sources such as explosive generators, which are a compact, energy-rich power source.

Gyrotrons are an extraordinarily mature source for high-average-power application at the several-megawatt level to the problem of heating magnetic fusion plasmas at electron cyclotron resonance frequencies of 100 GHz or more (see Chapter 3). In fact, gyrotrons join klystrons as the only sources that are produced to continuously generate power levels at 1 MW or above. Another variant of this class of *electron cyclotron masers*, the *gyroklystron*, has been investigated as an alternative to klystrons for power levels around 100 MW and frequencies in the X-band and above. Another variant, the *cyclotron*

autoresonance maser (CARM), potentially offers high power at high frequencies, since it features a linear upshift in frequency with beam energy, which compares to the quadratic frequency upshift of free-electron lasers without the complexity of wiggler magnets. In each case, however, these sources are immature at the gigawatt level, lacking the breadth and depth of development of other sources in comparable frequency ranges.

Free-electron lasers (FELs) are potentially the most flexible of all HPM sources, although they are also arguably the most complex. They offer almost unlimited frequency range, albeit at the expense of increasingly high beam energies as the frequency goes up. In one remarkable series of experiments, an FEL was operated at repetition rates of over a kilohertz, with power levels of the order of a gigawatt at frequencies over 100 GHz.

We include these sources in the book more for their strengths than their weaknesses. Current developments in virtual cathode oscillators may result in improvements in efficiency that make them more competitive with the sources treated in earlier chapters here. On the other hand, if future applications arise requiring the higher frequencies for which gyrotrons or ECMs and FELs are better suited, their importance in the field will increase.

10.2 Vircators

Virtual cathode oscillators are actually a class of sources that all depend on radiation generation by one or both of two phenomena that accompany the injection of an electron beam into a waveguide or cavity in which the beam current exceeds the local space-charge-limiting current: virtual cathode and electron reflex oscillations. Sources of this type include the *vircator, reflex triode, reditron, coaxial vircator,* and *feedback vircator* (or *virtode,* as it was originally known). These sources are capable of gigawatt-level output in the 1- to 10-GHz range of frequencies; they are relatively simple to build, since in many cases no magnetic field is required; and they generally operate at relatively low impedances, which makes them rather attractive from the standpoints of producing power at relatively low voltages and of coupling well to low-impedance power sources, notably compact, but single-shot, explosive electrical generators. They are also conspicuously tunable because their operation depends only on the charge density of the beam and not on any resonance condition. A single device can generate radiation over one or two octaves. The wide tunability of the vircator has made it a popular source in HPM testing facilities, where the variation of effects with frequency can be surveyed conveniently. Vircators with staggered tuning ranges have provided a testing capability from 0.5 to 10 GHz.[1] For all of these reasons, vircators are probably the most popular of HPM sources, with research or application efforts in all of the nations with HPM programs: the U.S. and Russia; France, Germany, the U.K, and Sweden; China and Japan; and relatively new nations to HPM, such as India, South Korea, and Taiwan. In a sense, for their simplicity and flexibility, vircators are the "starter source" for an HPM program.

Despite those advantages, these sources have historically suffered from relatively low efficiency, and they have been very sensitive to the problem of gap closure, which causes the diode current to increase with time, so that the frequency chirps upward, upsetting the balance between resonances in a way that causes output to drop (see Problem 1). These problems are being addressed particularly in the development of the coaxial and feedback vircators, so that these sources are currently enjoying something of a renaissance, which may cause their fortunes to rise again in the future.

10.2.1 Vircator History

As recounted in the review of Birdsall and Bridges, the Child–Langmuir relation for charged-particle flow in a diode traces to the early 20th century.[2] In the 1960s and 1970s, studies of virtual cathode formation by beams exceeding the space-charge-limiting current showed that the virtual cathode was unstable and quantified the dependence of the oscillation frequency and position of the virtual cathode on the experimental parameters. Sullivan et al. reviewed the development of vircator theory,[3] while Thode reviewed experiments[4] as of 1987.

A number of early experiments used the reflex triode configuration, in which the anode is pulsed positive and the cathode is grounded. In 1977, Mahaffey and coworkers were the first to produce microwaves using virtual cathode oscillation,[5] followed a year later by the publication of results from a group at the Tomsk Polytechnic Institute in Russia.[6] A group at Harry Diamond Laboratories (HDL) produced gigawatt output in the X-band with a reflex triode in 1980.[7]

The standard vircator, with its negative pulsed cathode and grounded anode, became more popular in the 1980s: Burkhart at Lawrence Livermore National Laboratory (LLNL) reported 4 GW at 6.5 GHz in 1987,[8] Bromborsky et al. at HDL recorded average peak power (averaging out spikes) of 9 GW at frequencies below 1 GHz in 1988 on the 6-MV AURORA accelerator,[9] and Platt et al. at the Air Force Weapons Laboratory (AFWL; now the Air Force Research Laboratory) achieved 7.5 GW at 1.17 GHz in 1989.[10] Two modifications of this basic design demonstrated increased efficiency. The *reditron,* proposed by Kwan and Thode at Los Alamos National Laboratory (LANL) from an earlier suggestion by Sullivan, employed a special anode design to eliminate reflexing by a thin annular electron beam to produce 3.3 GW at 2.15 GHz with a sharper frequency spectrum and an efficiency of about 10%,[11] significantly higher than earlier experiments at that time outside the U.S.S.R. The use of a double anode at LLNL, described in 1991, similarly increased device efficiency by synchronizing, rather than eliminating, electron reflexing with the oscillation of the virtual cathode.[12]

In 1987, Benford and coworkers at Physics International (PI; now L-3 Communications Pulse Sciences)[13] and Sullivan[3] introduced the *cavity vircator* and showed that virtual cathode interaction within a microwave cavity could eliminate mode competition and increase efficiency. Sze and coworkers at PI,[14] as well as Fazio et al. at LANL,[15] used a cavity vircator to achieve about a 5-dB amplification of the output of a relativistic magnetron in 1989. In 1990, Price and Sze phase locked a two-vircator array to the output of a relativistic magnetron operating in the S-band,[16] and Sze and others locked two-cavity vircators to one another, producing about 1.6 GW of total output.[17]

The *virtode* or *feedback vircator* was described in a 1993 publication from a group at the Kharkov Physico-Technical Institute.[18] This variation uses feedback from the microwave generation region through a waveguide back to the diode region where the electron beam is generated. Tunable versions of varying design spanned the frequency spectrum from the S- to the X-band at power levels up to 600 MW and efficiencies that ranged from 3 to 17%. More recently, Kitsanov et al. from the Institute of High-Current Electronics (IHCE) in Tomsk built a 1-GW S-band device of this type.[19]

In 1997, the *coaxial vircator*, in which the virtual cathode is generated by propagating a high-current electron beam radially inward, was proposed in computer simulations from Woolverton et al. at Texas Tech University,[20] followed by a later publication describing experiments.[21]

10.2.2 Vircator Design Principles

A virtual cathode is formed when the magnitude of the current I_b of an electron beam injected into a drift tube exceeds the space-charge-limiting current I_{SCL}. When a virtual cathode is formed, two things happen: (1) the location of the virtual cathode oscillates back and forth at roughly the beam plasma frequency ω_b, and (2) some electrons are transmitted through the virtual cathode while some are reflected back toward the diode, where eventually they are reflected by the cathode potential back toward the virtual cathode, an oscillatory effect known as reflexing. In general, the virtual cathode oscillation occurs at a different frequency than the reflex oscillations, although the two can be tuned to coincide, as we shall see.

Expressions for I_{SCL} were given in Chapters 4 and 9 in Equations 4.115 and 9.3a for a thin annular beam, Equation 4.116 for a beam with a uniform distribution across a circular cross section, and Equations 9.35 and 9.36 for a thin annular beam inside a coaxial drift tube. The general form for I_{SCL} is

$$I_{SCL}(kA) = \frac{8.5}{G}\left(\gamma_0^{2/3} - 1\right)^{3/2} \tag{10.1}$$

where γ_0 is related to the anode–cathode voltage in the electron beam diode V_0,

$$\gamma_0 = 1 + \frac{eV_0}{mc^2} = 1 + \frac{V_0(kV)}{0.511} \tag{10.2}$$

and G depends on the geometry. For example, for a thin annular beam of mean radius r_b within a circular-cross-section drift tube of radius r_0,

$$G = \ell n\left(r_0 / r_b\right) \quad \text{(annular beam)} \tag{10.3a}$$

whereas if the beam is uniformly distributed across the whole beam radius r_b,

$$G = 1 + \ell n\left(r_0 / r_b\right) \quad \text{(solid beam)} \tag{10.3b}$$

(see Problems 2, 3, and 5). Alternatively, if we have a thin annular beam within a coaxial drift tube of inner radius r_i and outer radius r_o, then

$$G^{-1} = \frac{1}{\ell n\left(r_o / r_b\right)} + \frac{1}{\ell n\left(r_b / r_i\right)} \quad \text{(annular beam, coaxial drift tube)} \tag{10.3c}$$

When $I_b > I_{SCL}$, a virtual cathode is formed and oscillates about a position at a distance downstream of the anode roughly equal to the anode–cathode spacing. The potential fluctuations at the virtual cathode produce a beam with an oscillating current density downstream of the virtual cathode, as well as a fluctuating current that is sent back toward the anode. The operation of a virtual cathode oscillator is best seen in computer simulations. Figure 10.1 shows the time dependence of the position and potential of a virtual cathode formed by a solid-cross-section beam injected through a foil anode into a cylindrical drift space.[22] The spikes in position generate a frequency spectrum that peaks at 10.4 GHz but contains many components. Broadband radiation is a basic characteristic of the simple vircator. We see the oscillation of the virtual cathode about a mean distance somewhat greater than the anode–cathode spacing, and a virtual cathode potential oscillation about a mean of roughly V_0.

From the simulation of a different diode, Figure 10.2 shows, at a single instant in time, the real space and phase-space positions of particles in a particle-in-cell simulation of a virtual cathode oscillator with no applied magnetic field.[4] The cathode on the left is a thin cylinder of metal projecting from a metal stalk; note that there is electron emission from the sides as well as from the tip of the thin cylinder at z = 1.50 cm. In the lower phase-space plot, we see that the electrons reach their maximum axial momentum, labeled P_z, at the location of the anode at z = 2.25 cm, and they decelerate as they propagate farther along the axis. We see that some stop, with $P_z = 0$ at the

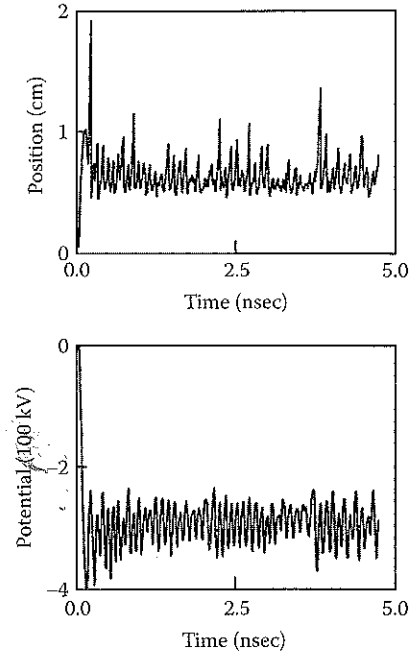

FIGURE 10.1
Time histories of the virtual cathode position and the magnitude of the virtual cathode potential obtained from computer simulation of a 270-kV, 7.3-kA beam of solid cross section and radius 1.25 cm injected through the anode of a diode with a 0.25-cm anode–cathode gap into a drift tube of radius 4.9 cm. (From Lin, T. et al., *J. Appl. Phys.*, 68, 2038, 1990. With permission.)

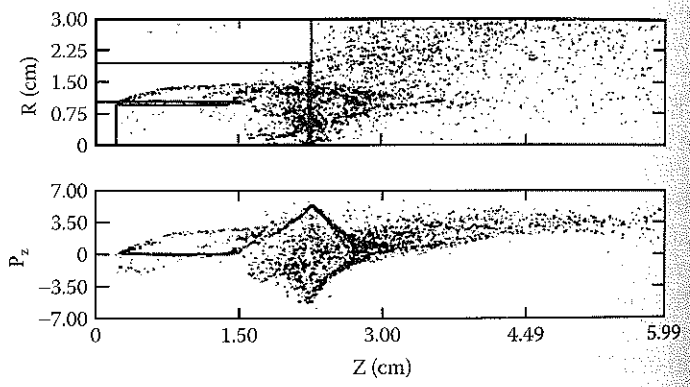

FIGURE 10.2
An r-z plot (top) and phase-space plot (bottom) of an electron beam forming a virtual cathode when injected into a drift space without an axial, guiding magnetic field. (From Thode, L.E., *High Power Microwave Sources*, Granatstein, V.L. and Alexeff, I., Eds., Artech House, Boston, 1987, p. 507. With permission.)

virtual cathode located at about z = 3.00 cm, returning into the gap with negative axial momenta. Those electrons do not reach the cathode because of the energy loss in the foil cathode. Clearly, though, many of the electrons are transmitted through the virtual cathode to pass down the drift tube with a substantial spread in axial momentum.

Virtual cathode oscillations occur at approximately the relativistic plasma frequency

$$f_p = \frac{1}{2\pi}\left(\frac{n_b e^2}{\varepsilon_0 m \gamma_0}\right)^{1/2} = 8.98\times10^3\left[\frac{n_b\left(cm^{-3}\right)}{\gamma_0}\right]^{1/2} \text{ Hz} \tag{10.4}$$

where n_b is the density of electrons in the beam as it passes through the anode, –e and m are the charge and mass of an electron, and ε_0 is the permittivity of free space. In practical units, we find

$$f_p\left(GHz\right) = 4.10\left[\frac{J\left(kA/cm^2\right)}{\beta\gamma_0}\right]^{1/2} \tag{10.5}$$

where $\beta = v_b/c = (1 - 1/\gamma_0^2)^{1/2}$, with v_b the electron velocity (see Problem 4). In the nonrelativistic limit, where $\gamma_0 \cong 1$ and $\beta \propto V_0^{1/2}$, Equation 4.1014 shows that $J \propto V_0^{3/2}/d^2$, so that

$$f_{VC} \propto \frac{V_0^{1/2}}{d} \quad \text{(nonrelativistic)} \tag{10.6}$$

In the strongly relativistic limit, on the other hand, when $\gamma_0 \propto V_0$, $\beta \cong 1$, and, according to Equation 4.107, $J \propto V_0/d^2$, so that

$$f_{VC} \propto \frac{1}{d} \quad \text{(strongly relativistic)} \tag{10.7}$$

This strongly relativistic regime is reached for higher voltages than we would normally encounter in an HPM system, but the point is that the voltage dependence weakens for voltages significantly above 500 kV. In addition to the oscillation of the virtual cathode itself, trapped electrons reflexing in the potential well formed between the real and virtual cathodes are bunched and consequently radiate at a reflexing frequency

$$f_r = \frac{1}{4T} = \frac{1}{\left(4\int_0^d \frac{dz}{v_z}\right)} \tag{10.8}$$

where d is the anode–cathode gap. In practical units, using the nonrelativistic expression for v_z in the anode–cathode gap,

$$f_r\left(GHz\right) \cong 2.5\frac{\beta}{d\left(cm\right)} \quad \text{(nonrelativistic)} \tag{10.9}$$

(see Problem 6). At relativistic voltages, because the electron velocity approaches the final value of βc more quickly, the multiplier approaches the limiting value of 7.5 (at which $v_b = \beta c$ all the way across the gap). The scaling of both f_{VC} and f_r is similar in the nonrelativistic regime, both frequencies falling within the microwave range, so that both phenomena are available to compete with one another. Generally, $f_{vc} > f_r$, and typically $f_{vc} \sim 2f_r$. As we shall discuss, configurations have been explored that either eliminate or exploit this competition.

Weak voltage scaling and the inverse scaling with d, which is the same in either the nonrelativistic or strongly relativistic cases, were confirmed in early experiments.[5] Later experiments by Price et al.[23] verified the inverse scaling with the anode–cathode spacing over a very wide frequency range, as shown in Figure 10.3. The data in the figure were obtained with a vircator that was tunable over about an order of magnitude, albeit at reduced power, as the frequency was extended down to about 400 MHz.

Woo used a two-dimensional treatment to find the beam plasma frequency for a pinched solid beam.[24] His treatment was based on the observation that a relatively low-current beam would not pinch, diverging to the wall and skirting the potential minimum established in the center of the drift tube that would cause reflection of electrons back toward the diode and formation of the virtual cathode. Following the history of the voltage and current during the course of a pulse, he showed that microwave emission began shortly after the time when pinching became significant — determined when the radial and axial current densities in the beam became equal — and that emission terminated around the time that the pinching became so strong that the radial current density became much larger than the axial current density, which is supported by experiments.[25] Using a formalism similar to that of Goldstein et al. for pinched-beam diodes[26] and Creedon for parapotential flow,[27] he derived an expression for the beam plasma frequency that agreed very well with experimental data:

$$f = \frac{c}{2\pi d}\ell n\left[\gamma_0 + \left(\gamma_0^2 - 1\right)^{1/2}\right] = \frac{4.77}{d\left(cm\right)}\ell n\left[\gamma_0 + \left(\gamma_0^2 - 1\right)^{1/2}\right] \text{ GHz} \tag{10.10}$$

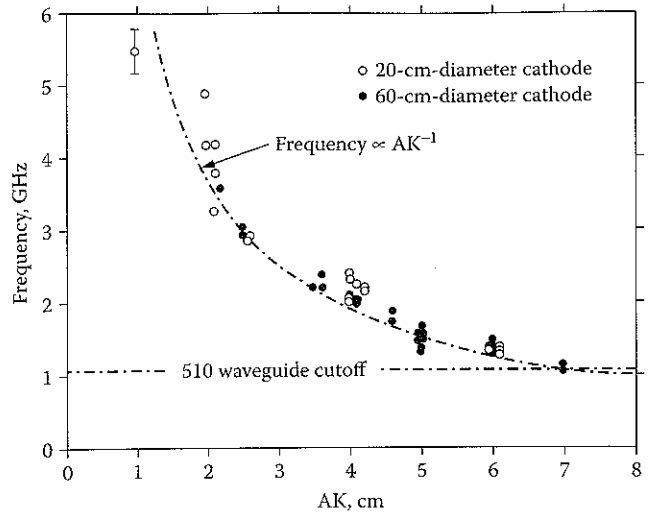

FIGURE 10.3
Tuning range of a vircator vs. the anode–cathode gap spacing, designated AK here (and d in the text). Cathodes of two different diameters were used, and power was extracted into WR-510 waveguide with the cutoff frequency shown. (From Price, D. et al., *IEEE Trans. Plasma Sci.*, 16, 177, 1988. With permission.)

This result is compared to data from a number of experiments in Figure 10.4 (see Problem 7).

In the absence of any downstream resonant structure, the bandwidth of the vircator is large because of several factors: nonuniform voltage, anode–cathode gap closure, and transverse beam energy. Since frequency depends on voltage and gap, the bandwidth is similarly dependent on variations in these two quantities. At nonrelativistic voltages, using Equation 10.6, we can see that

$$\frac{\Delta f_{VC}}{f_{VC}} = \frac{\Delta V_0}{2V_0} - \frac{\Delta d}{d} \tag{10.11}$$

The variation with the anode–cathode gap width d leads to *chirping* of the microwave frequency in diodes when the gap plasma causes closure, so that $\Delta d < 0$. Chirping is the phenomenon whereby the frequency climbs during the course of a pulse, in analogy with the chirp of a bird; the strongest chirping occurs at the highest frequencies, where gap closure is proportionately larger. Chirping results in a lower efficiency and lower gain because (1) the gain–bandwidth product is fixed for a given device with a fixed load and (2) the frequency changes so rapidly that the process generating microwaves does not fully establish itself before the resonant frequency shifts. The introduction of a resonant cavity downstream has been shown to improve the gain and narrow the bandwidth.

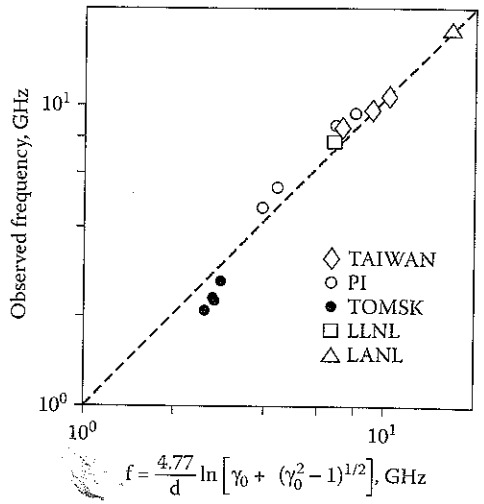

FIGURE 10.4
Comparisons of observed vircator frequencies with the two-dimensional analytic model of Woo. (From Woo, W.-Y., *Phys. Fluids*, 30, 239, 1987. With permission.)

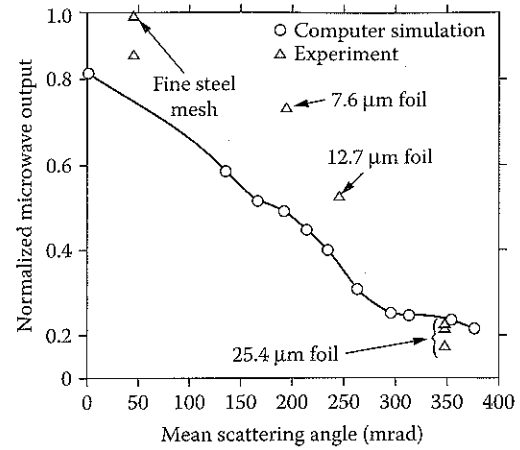

FIGURE 10.5
Decline of microwave power with scattering in the anode. Work done under the auspices of the University of California Lawrence Livermore National Laboratory, Department of Energy. (From Burkhart, S. et al., *J. Appl. Phys.*, 58, 28, 1985. With permission.)

Beam temperature, from both axial and angular variations in beam electron velocities, also broadens the bandwidth because the transverse components of the electrons' energy do not interact with the virtual cathode. Beam temperature is produced by both the emission process and scattering in the anode foil. Beam temperature also reduces radiation efficiency. The reduction in output power with beam temperature is illustrated in Figure 10.5, in which increasing the thickness of the anode, through which the beam passes, increases beam temperature by increasing the scattering angle of the electrons.[28]

Because the radio frequency (RF) field components excited by the vircator process are E_z, E_r, and B_θ, the modes excited are TM_{on}. The preferred mode appears to be near cutoff, i.e., the lower-order modes $n \sim 2\, r_a/\lambda$.

Foil-less diodes can also be used for vircator generation as long as the space-charge limit is exceeded. Because foil-less diodes have $\omega_p \approx \omega_c$, the electron cyclotron frequency, due to the presence of an axial magnetic field, foil-less diode vircators can be tuned in frequency simply by changing the magnetic field. The foil-less diode also offers advantages in reduced gap closure and flat impedance characteristics.

10.2.3 Basic Vircator Operational Features

The vircator domain of frequency operation extends from 0.4 to 17 GHz. Lower-frequency devices have larger dimensions. For example, Price et al. have reported a device that operates as low as 0.5 GHz with a chamber inner diameter of 80 cm and a cathode with a 60-cm diameter.[23] A 17-GHz vircator, by comparison, used a 6-cm chamber with a 2-cm cathode.[29] Low-frequency operation historically required the use of a velvet-covered cathode. Extrapolation to higher frequencies has been limited by plasma closure caused by the small gaps necessary to produce the very high current densities (see Problem 1). Pulse durations have typically been short (~50 nsec), but the Tomsk group[30] and Coleman and Aurand[31] have reported long-pulse experiments. Burkhart reported 4 GW in the C-band.[8] Platt and coworkers have reported 7.5 GW at 1.17 GHz,[10] and Huttlin and coworkers[32] have reported power in excess of 10 GW below 1 GHz. At the high-frequency end, Davis and coworkers[29] have reported 0.5 GW at 17 GHz.

The two basic vircator geometries for axial and side extraction are shown in Figure 10.6. In the axial vircator, the space-charge cloud couples to radial and longitudinal electric field components, giving TM modes that are extracted along the cylindrical waveguide, usually to a flared horn antenna. Early axial extraction experiments reported a gigawatt at the X-band.

The transverse or side-extracted vircator allows extraction in the TE_{10} mode. The beam is injected through the long wall of a rectangular waveguide forming a virtual cathode. The electric field between the anode and cathode is parallel to the small dimension of the waveguide. Thus, the electric field along the potential well of the virtual cathode system is parallel to the electric field of the TE modes of the waveguide. The rectangular waveguide is overmoded for the frequencies extracted. A remarkable feature of the side-extracted geometry is the purity of the TE_{10} mode; higher-order modes contribute less than 10% of the extracted power. Experiments by the PI group extracted a few hundred megawatts at efficiencies of about half a percent.[23,25] The most ambitious experiments of this type were conducted in the late

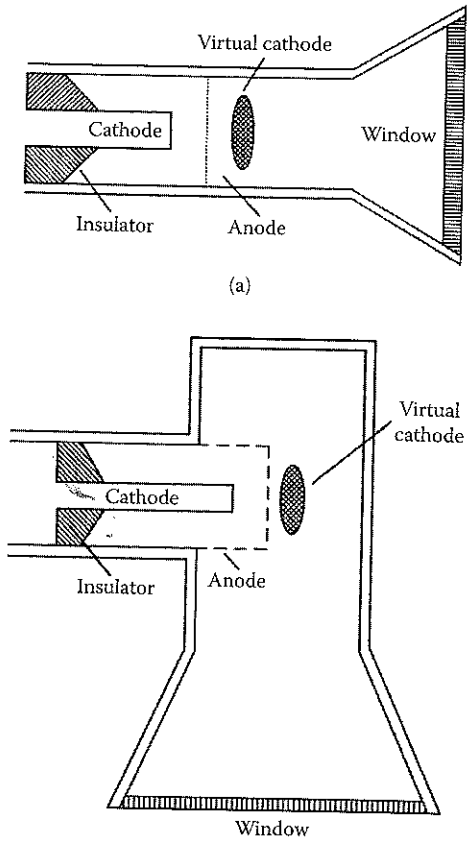

FIGURE 10.6
Basic vircator geometries: (a) axial extraction and (b) side extraction.

1980s at the Army Research Laboratory's now-dismantled Aurora facility. The best results were about 1 kJ in 18 radial arms at an efficiency of 0.6%.[32] The pulse was quite long, typically 100 nsec, with many spikes.

Figure 10.7 shows the basic reflex triode geometry. Note that in the reflex triode, the anode is the center conductor feeding the diode, and it is pulsed positive; by comparison, in vircators, the cathode is the center conductor, and it is pulsed negative. A reflex triode from the Grindsjön Research Center in Sweden, opened to the air, is shown in Figure 10.8.

Thode's survey[4] shows many common aspects of axial vircators. First, the radiation wavelength is typically

$$D < \lambda < 2D \tag{10.12}$$

where D is the waveguide diameter. Second, maximum power occurs with no applied axial magnetic field. If a thin anode is used with a guide field of

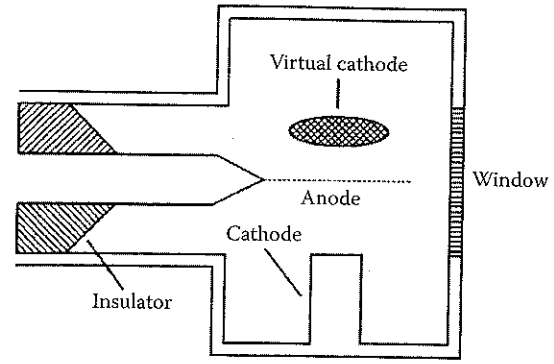

FIGURE 10.7
Basic reflex triode geometry.

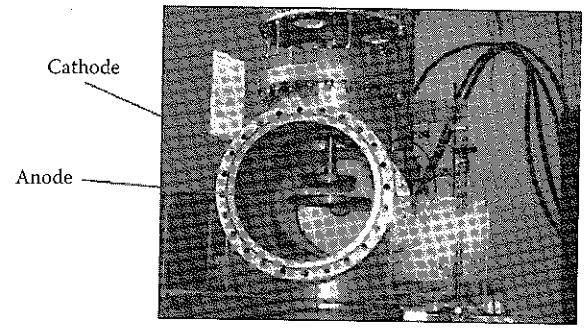

FIGURE 10.8
Side view of a reflex triode from the Grindsjön Research Center in Sweden, opened to the air.

~1 kG, little microwave radiation results. This indicates that two-dimensional motion in the potential well is important for microwave generation. However, the Tomsk and Livermore groups have observed high power at high magnetic fields (>5 kG). Poulsen et al.[12] of the Livermore group suggests that increasing the field in a device optimized for $B_z = 0$ simply moves away from a local optimum, reducing power, which can be recovered by reoptimizing geometry. Third, increasing anode thickness reduces microwave power if foil scattering reaches 300 mrad, as we showed in Figure 10.5. Fourth, microwave power depends strongly on the anode–cathode gap. If the gap is too small, the beam pinches and microwaves cease. If the gap is too large, approaching the cathode–wall separation, the beam expands to the outer conductor and is lost. At full-power tuning of the vircator is typically limited by these effects to a range of roughly one octave.

10.2.4 Advanced Vircators

Advanced vircators have been developed in two rather distinct periods. The reditron, the side-extracted vircator, the double-anode vircator, and the cav-

ity vircator were conceived and initially explored in the late 1980s to the early 1990s, while the virtode, or feedback vircator, and coaxial vircator are more recent innovations that are still in the active development stage. Of the three devices in the first generation, only the cavity vircator is still under development, and versions have been sold commercially.

10.2.4.1 Double-Anode Vircators

Researchers at Lawrence Livermore National Laboratory found that efficiency is increased when a resonance occurs in which the virtual cathode and reflex oscillation frequencies are equal, $f_{VC} = f_r$.[12] To achieve this, they employed the double-anode configuration of Figure 10.9 so that the two frequencies can be brought into equality by lengthening the transit time that determines f_r, as in Equation 10.8. Figure 10.10 shows that the resonant condition increases efficiency by about an order of magnitude. They report an output of 100 J from a single source with resonant conditions; however, the resonance condition is quite stringent. The bandwidth of high-efficiency operation was about 50 MHz, so that the frequencies must be equal to within 2%. Almost any diode closure defeated the resonance mechanism; the authors stated that variations of 100 μm in the anode–cathode gap significantly affected the output.

The Livermore group has attacked the problem of diode closure by using a variety of modified cathodes, the most successful being a field-enhanced thermionic emission cathode. They used a cathode with an area of 6 cm^2 with current densities from 200 to 300 A/cm^2 to produce microsecond pulse durations with no plasma formation enclosure. Unfortunately, at last reporting the device was not sufficiently reliable to produce sustained high-efficiency, long-duration microwave pulses with full-size cathodes.

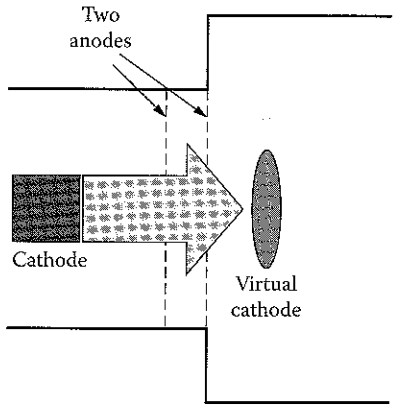

FIGURE 10.9
The double-anode configuration explored at Lawrence Livermore National Laboratory. The added travel time for reflexing electrons through the region between the two anodes is intended to synchronize the virtual cathode and reflex oscillations.

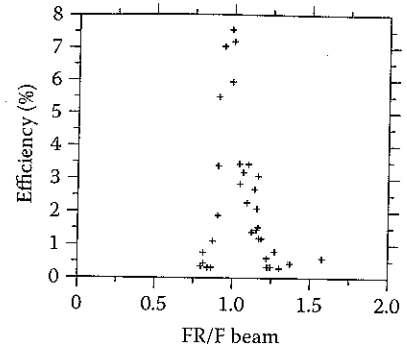

FIGURE 10.10
The resonant efficiency enhancement in the configuration of Figure 10.9 as a function of the ratio of f_r (designated FR in the figure) to f_{VC} (designated F beam in the figure). (From Poulsen, P. et al., *Proc. SPIE*, 1407, 172, 1991. With permission.)

10.2.4.1.1 Reditrons

An entirely different approach to the problem of competition between the virtual cathode and reflexing oscillations was taken at Los Alamos, where the reditron (for reflected electron discrimination microwave generator) was developed with the goal of completely eliminating electron reflexing.[11,29] The basic configuration of the reditron is shown in Figure 10.11.[33] The reditron features a thin annular beam and an otherwise thick anode with a thin annular cutout to allow the beam to pass out of the anode–cathode gap. An axial magnetic field guides the annular electron beam through the cutout in the anode to the downstream drift region. The part of the beam that reflects from the virtual cathode is no longer in force balance and expands radially; thus, it cannot pass through the annular slot and is absorbed in the anode. Reflexing electrons are almost eliminated, and only virtual cathode oscillations can produce radiation. In addition, the *two-stream instability* between outgoing and returning electrons is greatly reduced. When the streaming instability is present, electrons from the diode interact with returning electrons, and their angular divergence and energy spread are increased. Thus, their turning points in the virtual cathode's electric field are smeared out, which reduces the efficiency of the virtual cathode radiation mechanism.

Figure 10.12 shows a reditron configuration and phase-space diagram from a simulation by Kwan and Davis.[34] Compare this figure with Figure 10.2, which has no magnetic field and stronger counterstreaming electron interactions that cause much greater spreading of the electron beam. Simulations such as that in Figure 10.12 predict an efficiency of 10 to 20% and the production of narrow-bandwidth radiation (<3%); the oscillation frequency is ω_p. Since the reditron is an axial vircator, it creates TM modes, and simulations and experiments both show excitation of the lowest modes, typically TM_{01} or TM_{02}.

Elegant experiments by Davis and coworkers at Los Alamos verified the major features of the reditron concept.[33] Efficiency achieved in those exper-

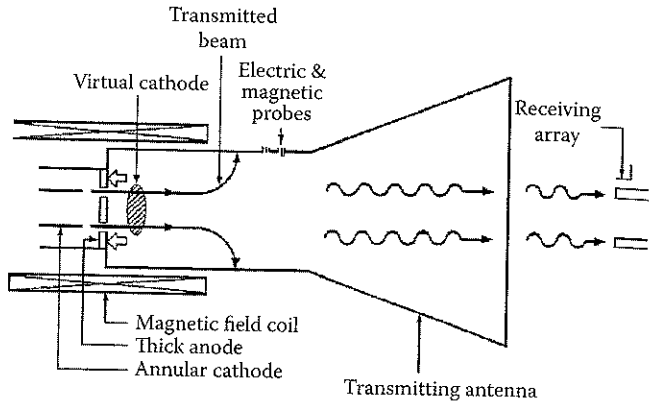

FIGURE 10.11
The reditron experimental arrangement. (From Davis, H. et al., *IEEE Trans. Plasma Sci.*, 16, 192, 1988. With permission.)

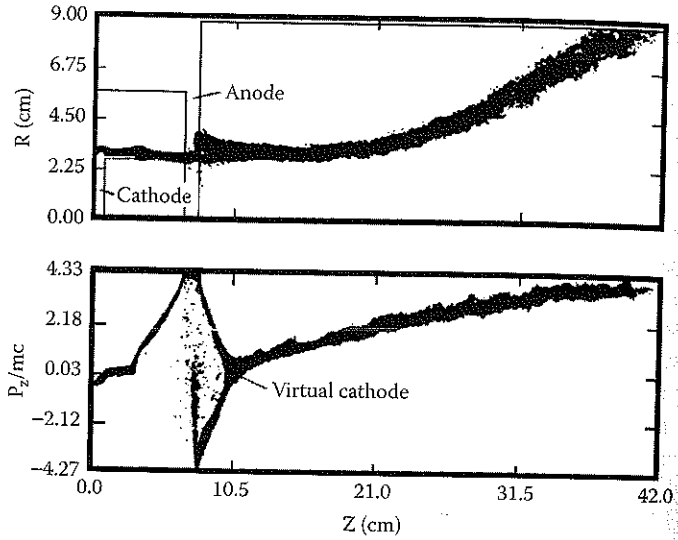

FIGURE 10.12
Simulation of a reditron experiment showing the formation of a virtual cathode, the loss of returning electrons on the thick anode, and the transmitted portion of the beam. (From Kwan, T.J. and Davis, H.A., *IEEE Trans. Plasma Sci.*, 16, 185, 1988. With permission.)

iments was 5.5 to 6%, compared to 1 to 3% when the apparatus was used in the conventional vircator geometry. Calculated diode and transmitted currents were 19 and 12 kA, very close to the measured values of 21 and 12.5 kA in the experiments. The beam current was verified to be the space-charge-limited value, I_{SCL}. Device impedances of 30 Ω to just over 60 Ω were seen in the experiments. Predicted power was 1.1 GW, compared to the 1.6 GW measured. Microwave power quenched well before the end of the electrical pulse. At lower powers, longer durations are observed, pointing to the possibility of breakdown processes. The observed frequency was 2.4 GHz with a bandwidth of 15 MHz, or less than 1%. Concentricity of the anode slot with the cathode was found to be essential for obtaining high power. Surprisingly, the highest power was produced when the beam just grazed the inside edge of the slot, rather than being centered in the slot. The data indicate that rapid diode closure or bipolar flow, due to the emission of ions from the anode, did not occur; the diode operated at constant impedance. Even in its initial experiments, the reditron showed great improvement in the fundamental vircator problems of efficiency, bandwidth, and chirping.

Computer simulations pointed to the possibility of further improvements on the reditron. The Los Alamos group showed that the oscillation of the virtual cathode can produce a highly modulated electron beam, with a modulation fraction as high as 100% occurring at the virtual cathode frequency.[35] Extraction of microwave power from this beam could enhance the output power and overall efficiency of the device. A straightforward way to extract the radiation is by use of an *inverse diode*. A center conductor is placed in the downstream waveguide, and it floats at a potential relative to the wall. The electron beam is absorbed in this conductor, a voltage then develops between the inner and outer conductors, and a TEM wave is transmitted along the coaxial line. Substantial radiation can be extracted downstream if the configuration is optimized. In the Los Alamos simulations, an inverse diode with a 50-Ω impedance was situated downstream of a reditron configuration. With a 1.2-MV diode, the kinetic energy of the leakage electrons impacting the center conductor was about 400 kV, with a highly modulated average current of 9 kA. The simulation gave an average peak power of 1 GW, so that the efficiency of the inverse diode was 28%.

Alternatively, the downstream region could contain a slow-wave structure. The premodulated electron beam from the vircator would induce wave growth at the modulation frequency.[36] This possibility was suggested by the Tomsk group.[37] Again, extraction downstream could increase overall vircator efficiency.

10.2.4.2 Cavity Vircators

A fundamental disadvantage of the vircator is that the downstream region in the basic vircator is large compared to the wavelength. The number of modes available in downstream waveguides or cavities allows many modes to be excited, so that as the vircator changes its characteristics due to variations in voltage or gap (Equation 10.11), there is always a waveguide mode at the appropriate frequency. The basic vircator also does not have one of the fundamental properties of most microwave devices, a feedback mechanism by means of a cavity to allow the field induced in the cavity by the oscillating virtual cathode to feed back on the virtual cathode, forcing it to oscillate at the resonant frequency of the cavity mode. Therefore, enclosing the vircator in a cavity has resulted in a fundamental improvement to the device.

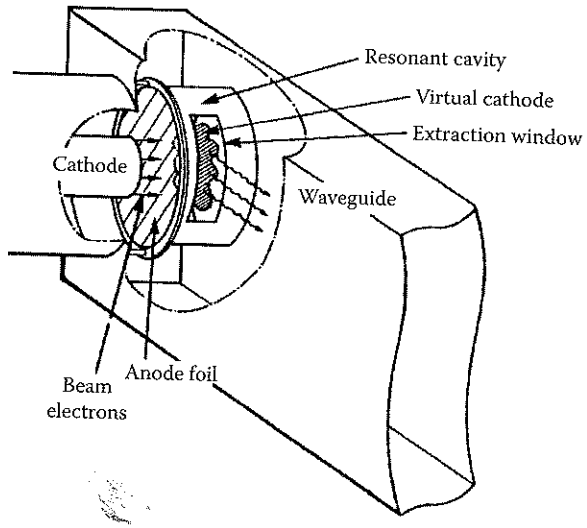

FIGURE 10.13
The resonant cavity vircator. (From Benford, J. et al., *J. Appl. Phys.*, 61, 2098, 1987. With permission.)

Of the many designs for cavities that could be considered, the pillbox cavity with a cylindrical cross section is the only one studied thus far because it is simple, has the same symmetry as the vircator itself, and is easily tuned by moving the end wall. The configuration chosen by the Physics International group (now L-3 Communications Pulse Sciences) in a transversely extracted vircator is shown in Figure 10.13.[13] In the first experiments, expendable aluminum cavities were used. The extraction window size was determined empirically, balancing the requirement for a large window to facilitate extraction and a small window to maximize the cavity Q. The window orientation shown in Figure 10.13 facilitates coupling to the fundamental TE mode of the rectangular extraction waveguide.

In cylindrical resonators, the TM modes are preferred, because E_z couples well to the virtual cathode electric field and B_θ allows convenient coupling through an output slot in the wall. The PI group found that the lowest-frequency TM_{010} mode required too small a cavity, so that the virtual cathode was shorted (the TM_{010} mode is also not tunable by varying the length). The experimental result was that the most tunable modes that were readily excitable were TM_{011}, TM_{020}, and TM_{012}. Perturbation by multiple output ports can influence the choice of mode.[38]

The effect of the cavity on the vircator output is shown in Figure 10.14. Total power in the initial experiments with cavity vircators was 320 MW with the cavity; to compare, the nonresonant cavity gave 80 MW. Another notable feature of the cavity is reduction in bandwidth by a factor of three. Spike structure in the output waveforms observed in earlier experiments, reflecting mode competition, was greatly reduced, and smooth pulse shapes were obtained. The cavity vircator is now a commercial product.

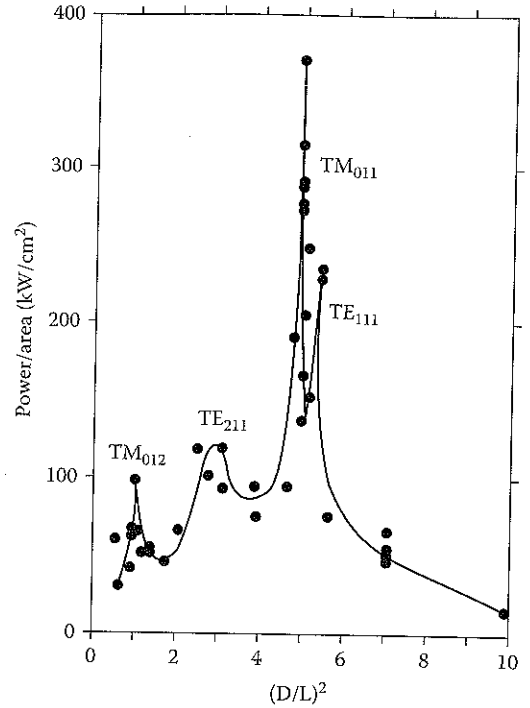

FIGURE 10.14
Radiated microwave power density as a function of the aspect ratio of a resonant cavity. Specific modes are identified. (From Benford, J. et al., *J. Appl. Phys.*, 61, 2098, 1987. With permission.)

The Los Alamos group has explored cavity vircators using a fixed cavity. Tuning is produced by varying the beam current density to bring ω_p in proximity to the passband of a suitable mode of the resonator. The TM_{020} and TM_{012} modes were excited with as much as a 70% variation in injected current.[39] A 1% bandwidth was obtained.

10.2.4.3 Virtodes and Feedback Vircators

In a sense, virtodes and feedback vircators strengthen the feedback mechanism used to increase power and narrow bandwidth in the cavity vircator. Rather than rely on the narrow frequency response of a cavity and the feedback mechanism of the reflexing electrons, the virtode, shown in Figure 10.15, feeds a portion of the microwave signal from the virtual cathode region directly back into the anode–cathode gap.[40] A device like that shown schematically in the figure was operated with a 450- to 500-kV electron beam at a current of up to 14 kA. An applied magnetic field of 0.2 to 0.6 T confined the beam and could be used to tune the output frequency. A maximum power level of 600 MW was achieved, and the efficiency ranged from 3 to 17%. Power without the feedback loop was at least a factor of two

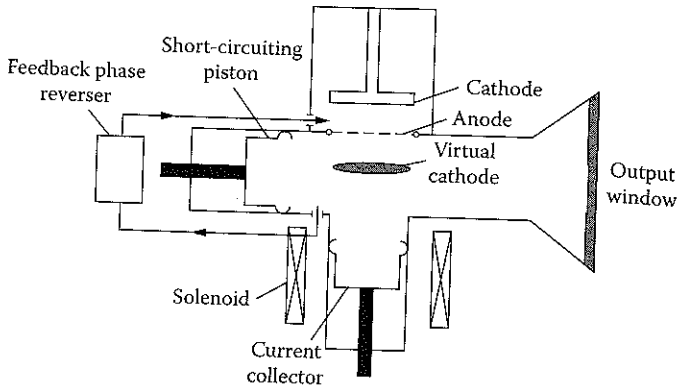

FIGURE 10.15
The virtode. (From Gadestski, P. et al., *Plasma Phys. Rep.*, 19, 273, 1993. With permission.)

smaller. By tuning the phase in the feedback circuit, the power output could be varied by as much as 5 dB. Tunability could also be effected by moving the current collector in and out. To capitalize on this mechanism, the movable current collector was replaced by a slow-wave structure with a beam collector downstream. In this geometry, the feedback loop into the diode gap was disconnected, but backard waves from the slow-wave structure could provide the necessary feedback. Power in this mode of operation reached 500 MW.

The feedback vircator of Figure 10.16 has been explored on both the SINUS-7 and MARINA generators at the Institute of High-Current Electronics in Tomsk.[41] On the latter, a compact inductive-storage machine with explosive fusing, a 1-GW, 2-GHz pulse of about 50-nsec duration was produced. With a voltage of about 1 MV and a current of about 20 kA, the efficiency was about 5%. The output was a quasi-Gaussian beam with the form of a TE_{10} mode. Ion emission in the diode was shown to cause electron beam pinching. By concentrating only on the portion of the beam current that was actually emitted from the cathode face, the authors inferred an effective efficiency of approximately 8 to 10%, closer to actual simulation results.

10.2.4.4 Coaxial Vircators

Coaxial vircators, originally developed at Texas Tech University, are the new entry into the field of advanced vircator development.[42,43] The basic configuration is shown in Figure 10.17. Note the cylindrical geometry and the fact that the electron beam propagates inward radially, taking advantage of the geometric convergence of the beam. The coaxial viractor is expected to have three advantages over traditional vircators. First, note that the anode–cathode region is not physically separated by conductors from the virtual cathode region to the interior of the anode. As a result, it is expected that the open geometry will allow feedback from the microwave generation region to the

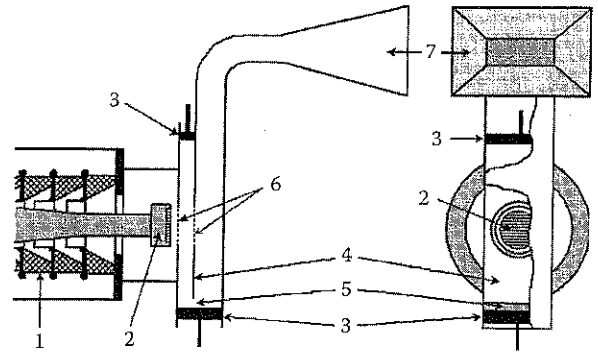

FIGURE 10.16
The feedback vircator used at the Institute of High-Current Electronics in Tomsk. (1) Stack-insulator interface to high-voltage generator, (2) bladed cold cathode, (3) tuning plungers, (4) partition wall, (5) coupling slot, (6) foil or mesh windows, and (7) vacuum horn. (From Kitsanov, S.A. et al., *IEEE Trans. Plasma Sci.*, 30, 1179, 2002. With permission.)

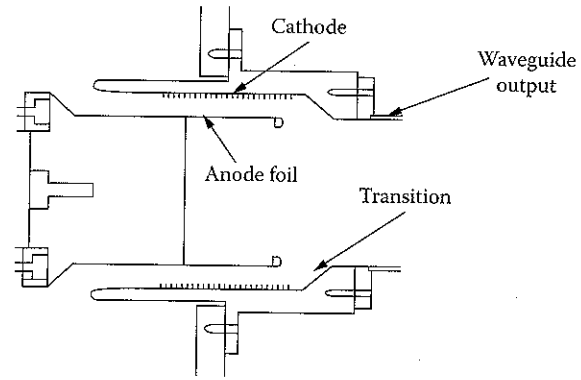

FIGURE 10.17
Side view of a cylindrical coaxial vircator.

beam. Second, the electron motion is radial only, eliminating the power loss associated with the axially transmitted portion of the electron beam in an axial vircator, as one can see in Figure 10.2 and Figure 10.12. Third, the large area of the diode reduces the current density and the beam loading of the cathode and anode, which is expected to increase the lifetime of the device, particularly under repetitive operation.

In the initial experiments, the cathode and anode radii were 13.1 and 9.9 cm; a 3-cm-long velvet cathode was the source of electrons. The diode was pulsed to 500 kV and a peak current of 40 kA for a 30-nsec pulse. The peak electron beam power was about 18 GW, while the peak microwave output was about 400 MW, so that the efficiency was about 2%. Remarkably, however, the microwave power pulse was offset and trailed the electron beam power pulse by about 10 nsec, so that the instantaneous power efficiency at

the time of peak microwave power appeared to be about 10%. The 2-GHz output was delivered in the form of a TE_{11} mode that was quite reproducible from shot to shot.

Coaxial vircators are a very active international research topic at this time. Despite the possible advantages of the device, several challenges remain to be solved: determining the optimum configuration; addressing the lack of tunability in current configurations; dealing with difficulties in alignment, particularly in repetitive operation; and addressing the serious mode competition between TE_{11} and TM_{01}.

10.2.4.5 *Phase Locking of Vircators*

Before closing this section, we return to the cavity vircator and consider the phase locking of these devices as an alternative, multisource path to high power. The next logical step beyond the cavity vircator was to inject an external signal into the cavity. Price and coworkers[14] injected the signal from a 100- to 300-MW relativistic magnetron into a vircator that was powered from the same electrical generator. The cavity vircator power varied from 100 to 500 MW. A striking result from this experiment was the extraordinary frequency pulling when the magnetron pulse was injected. When the vircator was radiating alone, the frequency dropped slowly due to gap closure, in good agreement with the two-dimensional model of Woo. The magnetron signal was injected at 2.85 GHz, and the vircator frequency, originally at 2.3 GHz, was pulled up to the magnetron frequency in about 10 nsec, an extraordinary range of frequency pulling. Of course, the injected signal was quite large.

Didenko and coworkers injected a conventional magnetron pulse into a reflex triode and observed about a 100-MHz frequency pulling, in agreement with a driven nonlinear oscillator model.[44] This result was also confirmed by Fazio and coworkers,[15] who reported a 250-MHz frequency pulling when a klystron injected into a vircator of roughly equal power. They also reported gain and linearity of vircator response so that this experiment could be described as a vircator-amplifier experiment with a gain of 4.5 dB. The PI group also reported amplification using a vircator driven by a magnetron.[14] With a drive power of 140 MW, as much as 500 MW was produced in a linear amplification mode.

The demonstration of phase locking of the vircator to an external signal shows that the vircator can be used in arrays, as can other oscillators, such as the magnetron.[14] To understand, recall Adler's inequality, which provides a condition on the phase difference between two oscillators that will permit phase locking. The important parameter is the injection ratio between power input, P_i, and power output, P_o:

$$\rho = \left(\frac{P_i}{P_o}\right)^{1/2} \tag{10.13}$$

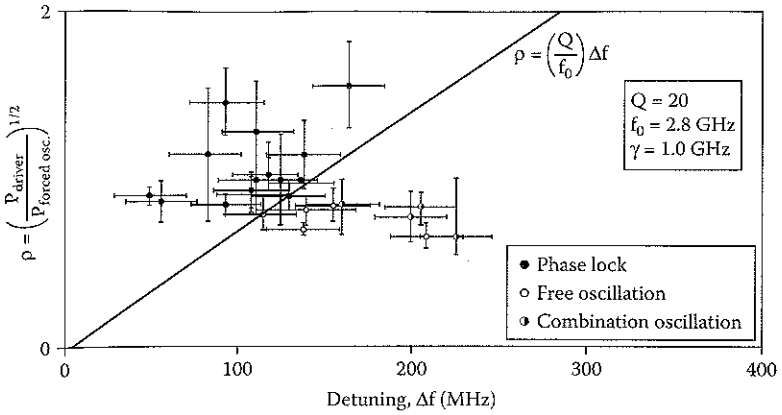

FIGURE 10.18
Adler relation for phase locking of a vircator to an external magnetron. Locked, unlocked, and combined states are shown. (From Price, D. et al., *J. Appl. Phys.*, 65, 5185, 1989. With permission.)

Phase locking occurs when the frequency difference between the oscillators is sufficiently small:

$$\Delta\omega \leq \frac{\omega_0 \rho}{Q} \tag{10.14}$$

where Q is the quality factor of the oscillators (assumed to be equal) and ω_0 is the mean frequency of the two oscillators. Figure 10.18 shows that Equation 10.14 is followed by the magnetron-driven vircator. In addition, there is an intermediate regime called a *combination oscillation* in which the vircator power output is modulated at a frequency corresponding to the frequency difference between the two oscillators. Price and Sze's theoretical analysis of the stability of the locking relation shows that the Adler inequality is a necessary but not sufficient criterion for phase locking.[45] Stable-locked steady-states are achieved in only a fraction of the parameter space. The stable regime occurs for $\rho \lesssim 1$. The rest of the Adler plane is unstable or unlockable. Therefore, overdriving an oscillator produces unstable oscillations and will not be observed as a phase-locked state. Moreover, the overall power of the system will be reduced.

Sze et al. demonstrated phase locking of two cavity vircators to one another.[17] Figure 10.19 shows their apparatus, in which a cathode stalk splits to feed two identical cylindrical cavity vircators, tunable with sliding end walls. Microwave generation starts once the diode currents exceed about 40 kA, about five times the space-charge-limiting current. The coupling bridge between the vircators is of length $7/2\ \lambda_g$, where λ_g is the waveguide wavelength at 2.8 GHz. The connecting bridge has a plunger that, when inserted, disconnects the cavities. The cavity frequencies can be tuned to within 20 MHz of one another. With the plunger withdrawn, the cavities mutually

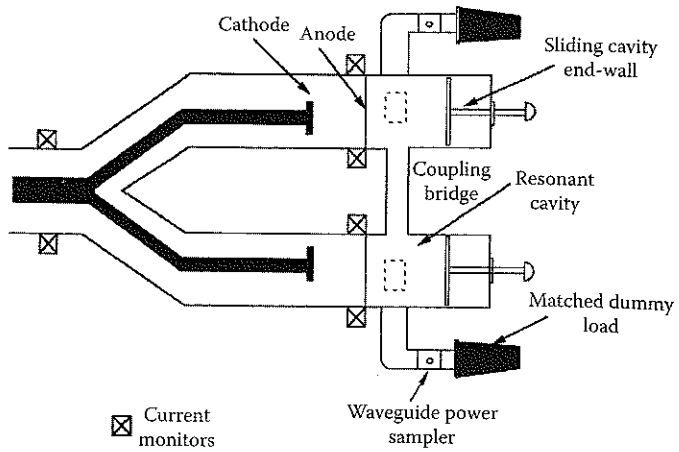

FIGURE 10.19
Dual-vircator phase-locking experiment. (From Sze, H. et al., *J. Appl. Phys.*, 67, 2278, 1990. With permission.)

couple and lock in less than 10 nsec. The relative phase angle varies from shot to shot by ±25°. There is some evidence that mode competition adversely affects the locking process; nevertheless, vircators were demonstrated to lock together in phase for about 25 nsec at a peak power level of 1.6 GW.

10.2.5 Fundamental Limitations and Outlook for Vircators

There will always be a place for vircators, in one form or another, in the field of HPM, because of their simplicity and ruggedness, tunability, versatility, and high power. Their ability to operate at low impedances — note that the Texas Tech coaxial vircator operated at less than 15 Ω — confers some advantage in specialized situations where the power source is an explosively driven flux compression generator with a low source impedance and a large amount of stored energy (see Figure 5.8). The limitation to date, and the question to be addressed by the relatively new cavity, tunable, and coaxial vircators, is the generally low efficiency of this class of devices. Beyond the untapped prospects for the new variants, it may be that some research group will return to some of the ideas explored for recovery of energy from the bunched transmitted beam using slow-wave structures or an inverse-diode arrangement.

10.3 Gyrotrons and Electron Cyclotron Masers

Gyrotrons and the associated class of *electron cyclotron masers* (ECMs), which includes *gyroklystrons* and *cyclotron autoresonance masers* (CARMs), tap the transverse energy of electrons that are gyrating about magnetic field lines. Although relativistic gyrotrons producing 100 megawatts have been explored experimentally, the primary driver for gyrotron development is for their application to magnetic confinement fusion research, where they provide megawatt-level, long-pulse (of the order of seconds to continuous) sources operating in excess of 100 GHz for electron cyclotron resonance heating, current drive, and suppression of instabilities.[46] High power gyroklystrons, approaching 100 MW, have been under development for years as an alternative source of X-band microwave power for radio frequency accelerators for electron-positron colliders. CARMs offer an alternative to free-electron lasers for using higher-energy electron beams to provide relativistic frequency upshifts to reach high power at high frequency. Other variants exist — gyro-BWOs, gyro-TWTs, large-orbit gyrotrons, peniotrons, and magnicons, notably — but none are being explored currently with a goal of producing truly HPM-level output.

10.3.1 History of Gyrotrons and Electron Cyclotron Masers

In the late 1950s, three investigators began a theoretical examination of the generation of microwaves by the electron cyclotron maser interaction:[47,48] Richard Twiss in Australia,[49] Jurgen Schneider in the U.S.,[50] and Andrei Gaponov of the U.S.S.R.[51] In early experiments with devices of this type, there was some debate about the generation mechanism and the relative roles of fast-wave interactions mainly producing rotational electron bunching and slow-wave interactions mainly producing axial electron bunching.[47,48] The predominance of the fast-wave ECM resonance with its rotational bunching in producing microwaves was experimentally verified in the mid-1960s in the U.S.[52] (where the term *electron cyclotron maser* was apparently coined) and the U.S.S.R.[53]

Gyrotrons were the first ECMs to undergo major development, and the requirement for high-average-power, continuous, or long-pulse millimeter-wave sources for electron cyclotron resonance heating, current drive, and instability suppression in magnetically confined plasmas for fusion research continues to drive the development of gyrotrons. As has been noted elsewhere,[54,55] early increases in device power were the result of Soviet-era Russian developments from the early 1970s in magnetron injection guns[56] to electron beams with the necessary transverse energy while minimizing the spread in transverse energies, and in tapered, open-ended waveguide cavities to maximize efficiency by tailoring the electric field distribution in the resonator.[57] Today, the production of megawatt-class gyrotrons at frequencies above 140 GHz has been the result of advances in mode control in extremely high-order-mode cavities, including the use of coaxial inserts; new internal mode converters to produce quasi-optical output coupling; depressed collectors to raise gyrotron efficiencies; and artificial diamond windows with the strength, low losses, and thermal conductivity to tolerate the passage of megawatt microwave output.[58]

The use of relativistic electron beams in gyrotrons followed shortly after the first relativistic beam-driven experiments with BWOs. The record for total output power from a relativistic gyrotron was the result of a collaboration between the Naval Research Laboratory (NRL) and Cornell University; in 1975, as much as 1 GW was reported by summing contributions from several frequencies between 8 and 9 GHz.[59] Gold et al. explored true HPM relativistic gyrotrons for a number of years at NRL as we shall discuss in Section 10.3.3.2. Their work resulted in the production of several hundred megawatts of output power in whispering-gallery devices operating near 35 GHz.

High power gyroklystrons operating in the X-band with power levels approaching 100 MW[60] were meant to provide a possible alternative to klystrons as drivers for a Next Linear Collider. This motivation for the development of these sources may change, however, with the 2004 shelving of the NLC concept in favor of the future International Linear Collider, which is to employ lower-frequency, lower-power RF sources.

Cyclotron autoresonance masers offer the possibility of tapping the large Doppler upshift of frequency afforded by relativistic beams in order to produce high power at high frequencies. Researchers at the Institute of Applied Physics in Nizhny Novgorod conducted the first investigations of these sources in the early 1980s,[61,62] but today they remain relatively immature sources that have not been fully explored.

Two other source types in this class appeared to hold out some promise for high power operation at one time, although they have not been brought to full maturity: quasi-optical gyrotrons and magnicons. Quasi-optical gyrotrons featured a large cavity resonator that was essentially open on the sides and bounded on each end by a mirror to form a Fabry–Perot resonator like that of an optical laser. The goal was to reduce the wall heating that plagued conventional gyrotrons. Originally proposed in the Soviet Union in 1967[63] and analyzed more extensively in the U.S. in the early 1980s,[64] these sources were investigated for a time at the NRL and the Ecole Polytechnique Federale de Lausanne in Switzerland, as well as at Yale University. Magnicons,[65] an enhancement of the original gyrocon,[66] are large-orbit devices originally proposed as drivers for the VEPP-4 accelerator at the Institute of Nuclear Physics in Novosibirsk. The interaction mechanism for these sources promised very high efficiencies, and although they were proposed for operation at tens of megawatts in the gigahertz range of frequencies, they have so far failed to fully realize their promise.

10.3.2 Gyrotron Design Principles

The typical configuration of a gyrotron, the most common type of ECM, is shown in Figure 10.20. Key features are the electron gun or diode, from which the beam is launched, the magnetic field and its axial profile, the interaction region or cavity, the beam collector, and the output extraction region. This diagram shows axial extraction, although as we shall see, side extraction with a mode converter has become far more common. A key

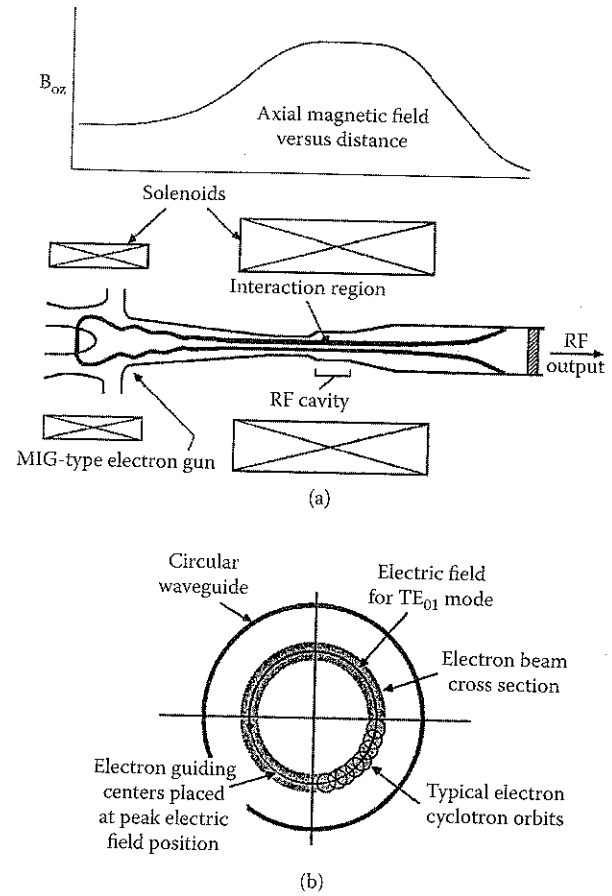

FIGURE 10.20
(a) Configuration of a gyrotron and the axial magnetic field profile. (b) The electron beam cross section showing some sample electron orbits within a gyrotron. (From Baird, J.M., *High-Power Microwave Sources*, Granatstein, V.L. and Alexeff, I., Eds., Artech House, Norwood, MA, 1987, p. 103. With permission.)

requirement of the electron beam in an ECM is that it have a specified value of the perpendicular velocity component. The ratio $\alpha = v_{0\perp}/v_{0z}$ at the entrance to the interaction region is an important parameter governing performance. As the beam moves downstream from the cathode, it is adiabatically compressed in a slowly increasing magnetic field, which raises the current density and increases $v_\perp$ as $B_{0z}^{1/2}$, the square root of the applied axial magnetic field, through the conservation of the electron magnetic moment,

$$\mu = \frac{\left(\frac{1}{2} m v_\perp^2\right)}{B_{0z}} \tag{10.15}$$

Naively, it might be expected that the largest possible value of $v_\perp$ would be desirable; however, in the magnetic compression process, if $v_\perp$ is too large, electrons will be reflected by *magnetic mirroring* if v_z is allowed to vanish (see Problem 8).

In long-pulse or continuous-wave (CW) gyrotrons, the magnetron injection gun (MIG), discussed at length by Baird,[54] is the most common beam source. In relativistic gyrotrons and CARMs, the electron beam is typically generated on an explosive emission cathode with much smaller perpendicular velocity components. Electron rotational energy can then be added after emission by passing the beam through a magnetic wiggler, like that used in an FEL, but short enough to not induce competing oscillations of its own, or through a single pump coil that introduces a nonadiabatic dip in the magnetic field and stimulates perpendicular electron velocity components.

Within the interaction region, the motion of the beam electrons decomposes into three components: a drift along the magnetic field v_z, a slow rotational motion of the beam as a whole about the magnetic axis of the system due to an $\mathbf{E} \times \mathbf{B}_0$ drift involving the radial self-electric field of the beam, and the Larmor rotation of the individual electrons at $v_\perp$ about their guiding centers. The minimum thickness of the beam is the Larmor radius of the electrons,

$$r_L = \frac{v_\perp}{\omega_c} \tag{10.16}$$

where ω_c is the electron cyclotron frequency,

$$\omega_c = \frac{eB}{m\gamma} \tag{10.17}$$

with γ the usual relativistic factor taking into account the total electron velocity (see Problems 9 and 12). Figure 10.20b depicts the rotational electron motion in a beam cross section.

In most cases, the ECM resonant interaction couples a transverse electric (TE) cavity mode to the fast Larmor rotation of the electrons. Signal gain from interactions with the transverse magnetic (TM) modes is also possible, but the coupling into TM modes in relativistic gyrotrons is reduced by β_z^2 relative to that for TE interactions, so that the TM interactions are overwhelmed in weakly relativistic devices. Nevertheless, a relativistic TM mode gyrotron has been built using a special resonator with enhanced Q for TM modes.[67]

The effect of the TE fields on a beamlet of electrons is shown in Figure 10.21.[68] In the figure, the electrons rotate counterclockwise in the x-y plane with a rotational frequency ω_c (we will ignore axial drifts without losing any of the important physics). Initially, as indicated in Figure 10.21a, they are

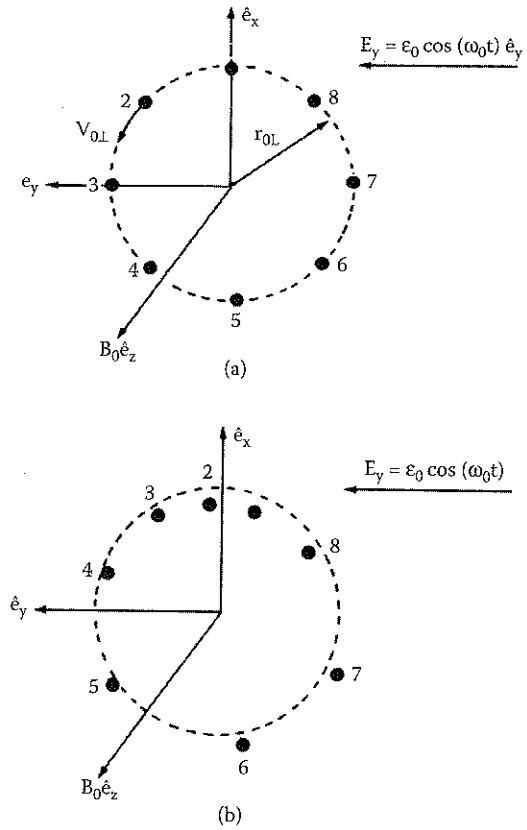

FIGURE 10.21
The bunching mechanism for eight test electrons. (a) The initial state in which the electrons are equally spaced in phase and executing Larmor rotations about a common guiding center. (b) After several cycles, the electrons have begun to bunch about the x-axis. (From Sprangle, P. and Drobot, A.T., *IEEE Trans. Microwave Theory Tech.*, MTT-25, 528, 1977. With permission.)

uniformly arranged in rotational phase on a circle with a radius r_L. The TE field with frequency ω_0 will first decelerate electrons 1, 2, and 8, causing them to lose energy and spiral inward; their rotational frequency, ω_c, will increase, though, because of the decrease in energy and the relativistic factor γ in the denominator of the expression for ω_c (Equation 10.17). Electrons 4, 5, and 6, on the other hand, will gain energy from the field, move outward, and rotate more slowly. Eventually, after a number of field periods, the electrons will bunch in rotational phase about the y axis. This effect, relativistic in origin due to the energy dependence of the rotational cyclotron frequency of the electrons, occurs for electron energies of even tens of keV. If $\omega_0 = \omega_c$, equal numbers of electrons are accelerated and decelerated, and no net energy is exchanged between the electrons and the field. On the other hand, if the oscillation frequency of the field exceeds the rotational velocity, $\omega_0 > \omega_c$, the situation is as depicted in Figure 10.21b, with more electrons

decelerated over a field period than are accelerated, and the electrons surrender net energy to the wave, which grows in amplitude. In a more general treatment with v_z taken into account, both azimuthal and axial bunching of the electrons occur. This situation simplifies with certain limits, however, as we shall see shortly. A number of mathematical treatments of gyrotrons and the instability underlying the operations of ECMs can be found in the literature (see, for example, Gaponov et al.[55] for a review of the early Soviet-era theoretical developments, and other references[68–72]).

Another generation mechanism, the Weibel instability, will compete with and, if the phase velocity of the electromagnetic modes in the interaction region is less than the speed of light, dominate the ECM instability.[73] There are devices in which some form of cavity loading is used to slow the waves and employ the Weibel instability as the generating mechanism.[74] Here, however, we will concentrate on fast-wave sources governed by the ECM interaction.

To estimate the operating frequency and illustrate the device types, we work with simplified dispersion diagrams for normal modes of the resonator, typically those of a smooth-walled-waveguide section with dispersion relations of the type given in Equation 4.19, for example, and the fast cyclotron waves on the electron beam

$$\omega = s\omega_c + k_z v_z \text{ , } s = 1, 2, 3, \ldots \tag{10.18}$$

where k_z and v_z are the axial wavenumber and axial electron drift velocity, and s in an integer, allowing for interactions at harmonics of the cyclotron frequency (see Problem 11). In fact, the space-charge on the beam and the nonzero $v_\perp$ split the fast cyclotron wave into a positive- and a negative-energy wave (just as space-charge splits the beam line in Cerenkov sources), with the higher-frequency wave of the pair being the negative-energy wave that interacts with the electromagnetic cavity mode to produce microwaves. Thus, their contributions raise the output frequency a bit above the approximate value given by Equation 10.18 (in contrast to Cerenkov sources, where generation occurs below the beam line). The point of intersection between the fast cyclotron wave and the cavity mode determines the type of ECM. Examples are shown in Figure 10.22. We distinguish three main types of devices involving forward-wave interactions in which the group velocity of the electromagnetic mode is positive at resonance. Gyrotrons operate near cutoff, gyro-TWTs have a somewhat larger value of k_z at resonance and a larger forward-directed group velocity at resonance, and CARMs have a large value of k_z and a substantial Doppler upshift in operating frequency (see Problem 14). The greatest gain usually occurs when the fast cyclotron mode intersects the electromagnetic mode tangentially on the dispersion diagram, so that the group velocity approximately matches the electron beam drift velocity. Hence, gyrotrons tend to use beams of lower axial energy in most cases. The greatest efficiency, on the other hand, occurs when the

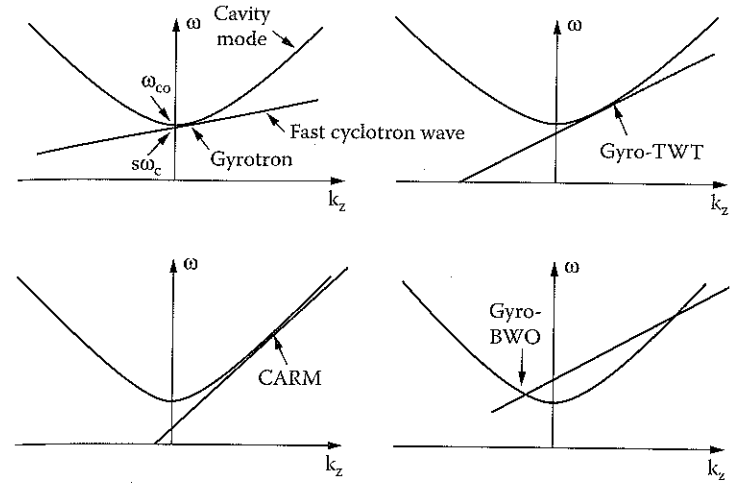

FIGURE 10.22
Dispersion diagrams for the uncoupled cavity mode, for which $\omega^2 = \omega_{co}^2 + k_z^2 c^2$, with ω_{co} the cutoff frequency for the operating mode, and the fast cyclotron wave on the beam, for which $\omega = s\omega_c + k_z v_z$, with ω_c the cyclotron frequency and s the harmonic number.

cyclotron frequency is detuned below the resonance line, so that the fast cyclotron mode line would actually lie somewhat below the line shown.

Historically, gyrotrons typically operated in one of the three types of modes depicted in Figure 10.23:[75] TE_{0p}, TE_{1p}, or a TE_{mp} mode with m >> p. This last type is known as a *whispering-gallery mode*, because its fields tend to be concentrated near the walls of the resonator, much like the acoustic whispering-gallery modes that carry sound near a wall. The TE_{0p} modes, with no azimuthal variation, have the smallest ohmic wall losses (see Figure 4.8). Unfortunately, the higher-order TE_{0p} modes suffer from mode competition, particularly with the TE_{2p} modes,[76–78] which impairs their ability to produce a high power signal. One method for selecting the desired mode under these circumstances is to use a complex cavity with two sections of different radii, essentially to constrain the oscillation to modes with a common frequency in both cavities.[79] The penalty for the use of such cavities is the increased space-charge depression of the beam energy accompanying the large radial separation between the beam and the wall in the larger of the two cavity sections. Another method for controlling the operating mode is to essentially split the cylindrical resonator along its sides to fix the azimuthal mode structure; the diffractive losses of modes with nonzero fields at the slits place them at a competitive disadvantage and effectively select the TE_{1p} modes.[80] The penalties for this method, however, are the somewhat higher ohmic wall losses for these modes, and the fact that their peak electric fields lie near the center of the cavity, so that good beam–field coupling, which requires the beam to be placed near the high-field region, implies substantial space-charge depression of the beam potential. Also, when the radial index p >> 1,

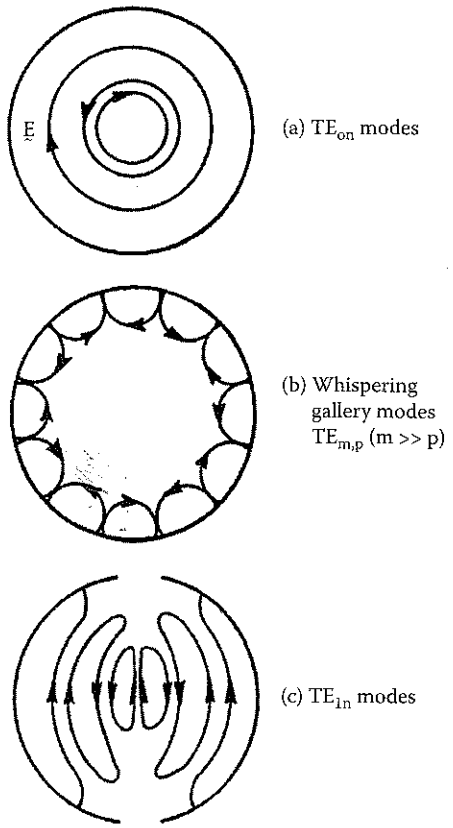

FIGURE 10.23
Three basic types of operating modes of a gyrotron. (From Granatstein, V.L., *High-Power Microwave Sources*, Granatstein, V.L. and Alexeff, I., Eds., Artech House, Norwood, MA, 1987, p. 185. With permission.)

the TE_{1p} modes become nearly degenerate in frequency. Finally, the slits fix the mode field pattern and do not allow it to rotate, so that portions of the beam couple poorly to the fields, and the efficiency is reduced.

In recent years, gyrotron designers have turned to high-order whispering-gallery modes for the operation of megawatt-class gyrotrons at frequencies above 100 GHz. For example, a 140-GHz, 1.5-MW gyrotron being developed at MIT for operation in several-microsecond pulses utilizes the $TE_{22,6}$ mode in a cylindrical interaction cavity.[81] On the other hand, a 165-GHz gyrotron being developed at FZK in Karlsruhe, Germany, as a prototype for an expected 170-GHz, 2-MW gyrotron to be required later focuses on a $TE_{31,17}$ mode in a coaxial interaction cavity.[82] In fact, design studies conducted in the early 1990s in Brazil at the Plasma Physics Laboratory at the National Institute for Space Research (São Jose dos Campos) even considered a $TE_{42,7}$ mode for a 1-MW, 280-GHz device (see Dumbrajs and Nusinovich[46]). The move to these very high order modes, in cavities that are 20 to 30λ in diameter, is driven primarily by the need to limit the thermal wall loading from cavity losses to 2 to 3 kW/cm².[58] Cavities simply must be large to have adequate wall area to handle the power loading, and the requirement for high-frequency operation creates the need to operate in a high-order mode. The whispering-gallery modes have several advantages in this regard.[83–85] Because their fields are concentrated near the walls, the electron beam must also be located near the wall to ensure good coupling. This factor reduces space-charge depression and related velocity spreads in the beam, enhancing efficiency; however, a large-diameter beam is therefore required, and minimizing beam losses to the cavity wall requires careful design. An additional advantage is that in this position, mode competition is reduced because of (1) the poor coupling to the volume modes with fields concentrated toward the interior of the cavity and (2) the relatively larger frequency spacing between other potentially competitive whispering-gallery modes.

The saturation of wave growth in ECMs is the result of two competing phenomena: depletion of the rotational energy and phase trapping.[68] For small values of $v_\perp$, depletion of the rotational kinetic energy is the dominant effect. Wave growth ceases when the perpendicular velocity component is reduced below the threshold for oscillation. When $v_\perp$ is large, on the other hand, the microwave fields build up to large amplitudes, and phase trapping is the dominant saturation mechanism. To explain, return to our discussion of the ECM interaction at the beginning of this section. Remember that some electrons are accelerated and some are decelerated by the fields. At the outset of the generation process, the signal frequency exceeds the cyclotron frequency of rotation, and more electrons are decelerated. As the electrons decelerate and their rotational phases change, the trapped electrons eventually reach a point at which further interaction with the fields causes some electrons to be reaccelerated. At this point, the electrons begin to take energy back from the fields, and the field amplitude passes through a maximum. This mechanism is phase trapping.[68] Figure 10.24, taken from the reference, shows the results of a numerical calculation of the microwave generation efficiency as a function of the initial relativistic factor. The authors of the paper assumed that all electrons had the same axial velocity, and the transformation was made to a moving coordinate frame in which the electrons had no axial drift velocity, only a rotational velocity; thus, $\gamma_{0\perp} = (1-\beta_{0\perp}^2)^{-1/2}$, with $\beta_{0\perp}$ the initial value of $v_\perp/c$. Shown also are two approximations to the efficiency based on rotational energy depletion and phase trapping. The minimum value for microwave generation to occur is $\gamma_{\perp,crit}$, ω_0 is the signal frequency, and $\Delta\omega$ is the amount by which the signal frequency should lie above ω_c in order for maximum signal growth to occur. The efficiency is maximum for an intermediate value of the rotational energy because of the combination of the two phenomena leading to saturation.

The perpendicular efficiency $\eta_\perp$ measures the microwave conversion efficiency from the electrons' rotational energy perpendicular to the magnetic field. This frequently quoted parameter must be distinguished, however, from the electronic efficiency for conversion of the total kinetic energy of the elec-